J. Sound Vib. (1971) 13 (4), 465–483

AEOLIAN TONES ASSOCIATED WITH RESONANT VIBRATION

P. LEEHEY AND C. E. HANSON

Acoustics and Vibration Laboratory, Massachusetts Institute of Technology, Cambridge, Massachusetts, U.S.A.

(*Received* 4 *November* 1969)

Measurements of oscillating lift coefficient, spanwise correlation length, Strouhal number, and radiated sound intensity were made on the same cylinder under the same test conditions over a Reynolds number range of 4000 to 6450. These measurements verified that the Curle theory of dipole radiation as expressed by Phillips for the Aeolian tone holds for a cylinder resonantly excited by a periodic wake in air. For small amplitude vibration, the increase of the oscillating lift coefficient with Reynolds number accounts for the increase of sound intensity.

1. INTRODUCTION

The study of the Aeolian tone has assumed added significance recently because of its role in the verification of the Lighthill–Curle theory of aerodynamic sound [1, 2]. By applying Curle's theory, Phillips [3] obtained a relation which gave the sound intensity and dipole radiation pattern from a rigid cylinder in a flow field. The effect of cylinder vibration did not enter the analysis directly although it was known long ago (Rayleigh [4]) that resonant vibrations reinforced the sound intensity considerably. Phillips reasoned that the effect of resonance would be to increase the spanwise correlation length of the shed vortices which, in turn, would increase the intensity of sound radiated.

On the other hand, Gerrard [5] found that if the cylinder is not resonantly excited, i.e. nearly rigid, the oscillatory sectional lift coefficient increased by two orders of magnitude over the Reynolds number range from 4×10^3 to 7×10^4 and stated that this effect alone was sufficient to explain the increase in radiated sound. A survey of measurements of correlation lengths by various techniques for supposedly rigid cylinders showed wide variations (Graham [6]), but the absence of any systematic increase of correlation length with Reynolds number in the transition region supported Gerrard's conjecture.

Evidence is developing that large phase correlations are directly associated with the "lock-in" effect where the frequency of vortex shedding is fixed to that of the resonant or forced cylinder vibration frequency (Koopman [7], Ferguson and Parkinson [8], Bishop and Hassan [9], and Berger [10]). The occurrence of "lock-in" and large phase correlation appears to require increasing vibratory amplitudes with increasing Reynolds number.

It is possible, by use of sufficient tension, to produce small resonant vibration amplitudes at Reynolds numbers in the transition region, even when the cylinder is lightly damped. The investigation reported here is concerned with this circumstance. Its purpose is twofold. First, it affords a means of direct experimental verification of the theory of aerodynamic dipole radiation on a single test apparatus. This is necessary for conclusive verification of the theory because of the extreme sensitivity of the essential parameters to variations in Reynolds

number or test environment (Lighthill [11]). Second, it provides further insight into the manner in which cylinder vibration interacts with the flow in the generation of Aeolian tones.

2. THE THEORY OF THE AEOLIAN TONE

The theory of aerodynamic sound is based upon the wave equation for the fluid density ρ

$$\nabla^2 \rho - \frac{1}{c_0^2}\frac{\partial^2 \rho}{\partial t^2} = -\frac{1}{c_0^2}\frac{\partial^2 T_{ij}}{\partial x_i \partial x_j},$$

where

$$T_{ij} = \rho u_i . u_j - \tau_{ij} - c_0^2 \rho \, \delta_{ij}$$

is the Lighthill stress tensor [1]. Here c_0 is the sound speed, $\mathbf{u}_i$ a velocity vector, τ_{ij} the stress in the fluid and δ_{ij} the Kronecker delta.

Using Kirchhoff's formula for the retarded potential and the momentum equations, Curle [2] obtained an exact expression for the flow exterior to a surface S,

$$4\pi c_0^2\{\rho(\mathbf{x}, t) - \rho_0\} = -\int_S n_i \left[\frac{\partial \rho u_i}{\partial t}\right]\frac{\mathrm{d}S(\mathbf{y})}{r} + \frac{\partial}{\partial x_i}\int_S n_j[\rho u_i . u_j - \tau_{ij}]\frac{\mathrm{d}S(\mathbf{y})}{r} +$$

$$+ \frac{\partial^2}{\partial x_i \partial x_j}\int_V [T_{ij}]\frac{\mathrm{d}V(\mathbf{y})}{r}, \tag{1}$$

where $r = |\mathbf{x} - \mathbf{y}|$, [ ] is the retardation operator $t \to t - r/c_0$ and $\mathbf{n}$ is the unit inward normal to S.

We may apply this result to determine the acoustic radiation from the periodic wake of a cylinder of length l and diameter d in a uniform flow of velocity $\mathbf{u}$ normal to the cylinder axis. We consider the cylinder to be a taut wire, hence incompressible, but capable of vibrating under the influence of the periodic wake with an amplitude s small compared to d. The fluctuating Reynolds stress $\rho u_i . u_j$ is assumed small compared to the actual stress τ_{ij} exerted by the surface S upon the fluid. We further assume that $r \gg \lambda \gg d$, where λ is the acoustic wavelength corresponding to the predominant frequency of the periodic wake. Hence the Mach numbers U/c_0 and s/λ are small. We may thus neglect the final quadrupole radiation term in (1) and assume $\rho \simeq \rho_0$ on S. The resulting linearized equation for the far-field radiation is (see Fitzpatrick and Strasberg [12])

$$\rho(\mathbf{x}, t) - \rho_0 \simeq \frac{1}{4\pi c_0^3}\int_{-l/2}^{l/2} \frac{\cos\theta_i}{r}\left[\rho_0 A \frac{\partial^2 \tilde{u}_i}{\partial t^2} + \frac{\partial f_i}{\partial t}\right]\mathrm{d}y_3,$$

where $\cos\theta_i = (x_i - y_i)/r$, $y_i = (0, 0, y_3)$, A is the cross-sectional area of the cylinder, $\tilde{u}_i$ is the velocity of the centroid of a cross-section and f_i is the force per length of the cylinder on the fluid.

If the cylinder is rigid, $\tilde{u}_i$ is zero and $-f_i$ is the fluctuating force per length of the wake on the cylinder. Over a wide range of the Reynolds number $\rho_0 Ud/\mu$, the wake is strongly periodic with a fundamental frequency ν given by a near constant value of the Strouhal number $S = \nu d/U$. We shall focus our attention on the fluctuating lift per length $-f_2$. We assume this to be a very narrow-band random process of average frequency ν, with a root-mean-square sectional lift coefficient

$$C_l = \frac{\rho_0}{2} U^2 d\overline{(f_2^2)}^{1/2}$$

and a random phase of vortex shedding along the cylinder characterized by an integral correlation length l_c and a centroid γ related to the moment of positive correlation area. Under the further assumption that $x = |\mathbf{x}| \gg l$ and $l_c \ll \lambda$, the intensity I of far-field radiation at frequency ν is (Phillips [3], Keefe [13])

$$I(x) = \frac{1}{16} \frac{\rho}{C_0^3} \frac{\cos^2 \theta}{x^2} C_l^2 U^6 (l - \gamma) l_c, \tag{3}$$

where θ is the polar angle of the observer at x from the normal to the cylinder axis and to the direction of the uniform inflow U. We have assumed the origin of the co-ordinate system to be located at the mid-span of the cylinder.

A fully satisfactory experimental verification of (3) has heretofore not been accomplished. Phillips [3] attempted an experimental verification using results from three separate experiments. A whirling arm device was used to determine the sound intensity I, the spanwise correlation length l_c was estimated from visual observation of the wake of a cylinder towed in water, the sectional lift coefficient C_l was inferred from Kovasnay's [14] measurements of the fluctuating velocities behind a cylinder. More refined experiments were performed by Keefe [13], but once again the data from three separate experiments were collected to verify equation (3). He measured the sound intensity I radiated from various cylinders in the flow of an open jet within an anechoic room. The lift coefficient C_l was measured on another cylinder in a closed test section of the subsonic wind tunnel at the University of Toronto Institute of Aerophysics, and spanwise correlation length l_c was taken from an average of pressure correlations on the surface of a cylinder by Prendergast [15] and velocity correlations near a cylinder by el Baroudi [16]. Because the quantities C_l, l_c and γ are strongly dependent on the Reynolds number, cylinder end conditions, upstream turbulence and cylinder vibration, these experiments afforded only a qualitative verification of equation (3). Lighthill [11] suggested that a satisfactory verification of the theory for a rigid cylinder would require that all quantities in equation (3) be measured on the same cylinder under the same test conditions.†

We have endeavored to carry out such a program, modified only by the observation that equation (3) should be valid for a vibrating cylinder in air provided that the radiation from vibration alone is insignificant compared to the radiation associated with oscillatory forces on the cylinder resulting from the periodic wake. Thus the root-mean-square sectional lift coefficient is determined by the wake forces alone, the force component due to cylinder motion being neglected. The influence of vibration upon the wake is not likely to be insignificant, however, and the effect of this upon radiated sound could be studied through changes in the quantities C_l, l_c and γ.

We shall be concerned with the vibration of a taut cylindrical wire in a uniform normal flow, particularly when the Strouhal frequency of vortex shedding is coincident with a resonant frequency of the wire. We shall also be concerned with the forced vibration of the wire by electromotive action at this resonant frequency in the absence of mean flow. If the damping at resonance is sufficiently small, and if we can neglect higher harmonic and broadband components of the excitations, the wire will vibrate in both cases in the corresponding

† While completing the writing of this paper, the authors became aware of a parallel investigation by Koopman [17]. Koopman performed an experimental verification of the near-field equation corresponding to our equation (2), using direct measurements of the total lift force on a resonantly vibrating cylinder. It appears, however, that he neglected to include the independent contribution from cylinder vibration, $\rho_0 A(\partial \tilde{u}_l / \partial t)$ in the near field. His calculated values of near-field sound pressure correspond rather well with measured values, however. This is not surprising in light of the fact, as we show later, that both the independent contribution from cylinder vibration and the component of total lift due to cylinder vibration yield small contributions to the acoustic field compared to that contributed by the lift from vortex shedding.

mode. If the same vibration amplitude is established in the two cases, C_l for the flow excitation can be determined by a comparison technique to be described more fully in the next section.

Let us identify the following cases:

case I, rigid cylinder with periodic wake flow of frequency ν;

case II, resonantly vibrating cylinder with periodic wake flow of frequency ν;

case III, resonantly vibrating cylinder driven electromagnetically at frequency ν to the same amplitude as in case II but with no mean flow.

In principle, equation (2) could be used to predict the acoustic radiation in all three cases. Equation (3), however, applies strictly to case I alone. Furthermore, both retarded terms of the integrand of equation (2) are dependent on $\tilde{u}_l$. If we can determine that the radiation associated with cylinder vibration is negligible compared to that associated with periodic wake forces on the cylinder, then equation (3) applies to case II as well.

Let us separate the fluctuating lift per length into a component $-f_2^{(e)}$ due to excitation plus a component $-f_2^{(v)}$ due solely to vibration. In case I, $f_2^{(v)}$ is zero, hence $-f_2 = -f_2^{(e)}$. In case II, we define $-f_2^{(e)} = -f_2 + f_2^{(v)}$, where $f_2^{(v)}$ is the same as for case III. We determined experimentally that the sound pressure level measured in the lift direction was at least 25 dB higher in case II than in case III. Thus in equation (2), for case II,

$$\rho_0 A \frac{\partial^2 u_2}{\partial t^2} + \frac{\partial f_2^{(v)}}{\partial t}$$

is negligible compared to

$$\frac{\partial f_2^{(e)}}{\partial t}$$

in determining the radiated sound. Hence equation (3) can be applied to case II provided the lift coefficient is determined from $-f_2^{(e)}$ as we have defined it.

In substantiation of our experimental result, a calculation of the radiation into an inviscid medium by a cylinder vibrating in a resonant mode was carried out, Appendix I. The cylinder was assumed simply supported between two semi-infinite rigid cylindrical baffles of the same radius. For conditions typical of our experiments, the radiation was found to be nearly end fire along the cylinder axis and of level no greater than measured in case III.

The comparison technique requires that the frequency response function of the cylinder be the same in cases II and III. Although the cylinder motion is essentially the same in the two cases, the presence of a mean flow in case II will alter the added mass, radiation damping and viscous damping from their case III values. Intuitively, we might expect these changes to be small. Our definition of the excitation for case II, however, avoids the necessity of estimating the changes, for it ensures that the frequency response function, although it cannot be calculated exactly, will be the same in the two cases.

We do assume that the quantities l_c and γ, which strictly speaking should be determined from the spatial correlation of $-f_2^{(e)}$, can be inferred from the spatial correlation of the longitudinal component of wake velocity. The physical plausibility of this assumption is reinforced by the fact that we have extracted those surface forces whose correlations would be unrelated to the wake.

For our experimental conditions in case III, an estimate of the radiation damping for inviscid flow is given in Appendix I and, following Batchelor [18], an estimate of the viscous damping for incompressible flow is given in Appendix II. (It is unnecessary to consider the more general viscous, compressible case as the Mach number s/λ is extremely small.) Both estimated values are very small compared to the measured total damping.

3. THE COMPARISON TECHNIQUE FOR MEASUREMENT OF THE SECTIONAL LIFT COEFFICIENT

From the arguments in section 2, we may write the dynamical equation for small vibration amplitude s of a wire under large tension T as

$$\rho\frac{\partial^2 s}{\partial t^2}+\rho\beta\frac{\partial s}{\partial t}-T\frac{\partial^2 s}{\partial z^2}=-f_2^{(e)}-f_2^{(v)}, \tag{4a}$$

where ρ is the mass per length of the wire, β is a material damping coefficient and $z=x_3$ is the spatial co-ordinate along the wire axis.

If the wire is resonantly excited at the same natural frequency to the same vibration amplitude with very small total damping in both cases II and III, we may include $f_2^{(v)}$ in the inertial and damping terms of the left-hand side of equation (4a) to arrive at

$$\frac{\partial^2 s}{\partial t^2}+\beta_t\frac{\partial s}{\partial t}-c^2\frac{\partial^2 s}{\partial z^2}=-\frac{f_2^{(e)}}{\rho_t}, \tag{4b}$$

where $c^2=T/\rho_t$ is the wave speed in the wire, ρ_t is the total mass per length of the wire including the inertial effect of fluid loading and β_t is an *ad hoc* damping coefficient representing the combined effects of material damping, vibratory power flow through the end supports and viscous and radiation damping. We emphasize here, from our arguments in section 2, that the response function of the wire, implicit in equation (4b), will be the same in cases II and III and that the excitation $-f_2^{(e)}$ in case II is the difference between the total fluid force on the wire and that which would be imposed if the wire vibrates as in case III. It is this excitation that yields the lift coefficient C_l required for the application of equation (3) to our experiments.

For very large tension T, non-linear effects due to fluctuations of tension with displacement s and stiffness effects near the end supports of the wire may be neglected and the wire will oscillate in the plane of the excitation (Miles [19]). If the transverse impedance of the end supports is also very large, we may, insofar as we are concerned with the wire, assume the end conditions to be †,

$$s(0,t)=s(l,t)=0. \tag{5}$$

The generalized Fourier transform of wire displacement is

$$\bar{s}(z,\omega)=\frac{1}{2\pi}\int_{-\infty}^{\infty}s(z,t)\,\mathrm{e}^{-\mathrm{i}\omega t}\,\mathrm{d}t.$$

The generalized Fourier transform of oscillatory lift per length $\bar{f}(z,\omega)$ is defined similarly. For case II, we consider the lift per length to be a stationary random process in z and t. We assume that the integral correlation length l_c is very much less than l. We further assume that the cross-spectral density,

$$\Phi_f(\zeta,\omega)=E\bar{f}(z,\omega)\bar{f}^*(z',\omega)\,\mathrm{d}\omega, \qquad \zeta=z'-z, \tag{6}$$

where E is the expectation and * denotes the complex conjugate (Cramér and Leadbetter [20]), is of the form

$$\Phi_f(\zeta,\omega)=\tfrac{1}{2}E(f^2)\,l_c\,\delta(\zeta)\{\delta(\omega-\omega_0)+\delta(\omega+\omega_0)\}. \tag{7}$$

Here δ is the Dirac delta function. The oscillatory lift per length is thus essentially pure tone at the frequency $\omega_0=2\pi\nu$ of vortex shedding, weakly phase-correlated along the wire axis.

† For convenience in this section we set the z-co-ordinate origin at one end of the cylinder.

The effects of deviations from these properties at the ends of the wire are considered negligible.

We expand $\bar{s}$ and $\bar{f}$ in terms of the orthonormal functions

$$\psi_n(z) = \sqrt{\frac{2}{l}} \sin \frac{n\pi z}{l},$$

as

$$\bar{s}(z, \omega) = \sum_{n=1}^{\infty} A_n(\omega) \psi_n(z)$$

and

$$\bar{f}(z, \omega) = \sum_{n=1}^{\infty} B_n(\omega) \psi_n(z).$$

The functions $\psi_n(z)$ are the normal modes of undamped free oscillation of the wire and hence satisfy the boundary conditions (5).

By elementary methods, we find that

$$A_n(\omega) = B_n(\omega)/W_n(\omega), \tag{8}$$

where, for $\beta = \eta|\omega|$,

$$W_n(\omega) = T\{k_n^2 - k^2(1 \pm i\eta)\}, \qquad k_n = n\pi/l, \qquad k = \omega/c, 0 \lesssim \omega.$$

The cross-spectral density of wire displacement is thus

$$\Phi_s(z, z', \omega) = E\bar{s}(z, \omega)\bar{s}^*(z', \omega)\,\mathrm{d}\omega \simeq \frac{\psi_n(z)\psi_n(z')E(f^2)l_c\{\delta(\omega - \omega_0) + \delta(\omega + \omega_0)\}}{2|W_n(\omega_0)|^2}$$

for loss factor $\eta \ll 1$, where $\omega_0 = 2\pi\nu = (1 - \eta^2/4)^{1/2} n\pi c/l$ indicating coincidence of the shedding frequency with the damped natural frequency of the wire in mode n.

The mean square value of any temporarily stationary quantity, linearly dependent on wire amplitude s, may be used as a comparison quantity to be matched with a case III experiment. If a steady magnetic field of flux $B(z)$ per length is impressed across the wire normal to the lift direction, a voltage

$$v(t) = -\int_0^l B(z) \frac{\partial s}{\partial t}(z, t)\,\mathrm{d}z$$

is generated in the wire. Writing $B(z)$ as a Fourier series,

$$B(z) = \sum_{n=1}^{\infty} D_n \psi_n(z),$$

we find that

$$E(v^2) = \frac{E(f^2) l_c \omega_0^2}{|W_n(\omega_0)|^2} D_n^2,$$

where

$$D_n = \int_0^l B(z)\psi_n(z)\,\mathrm{d}z.$$

Case III may be treated deterministically. Here,

$$f(z, t) = \sqrt{2}\, I_{\mathrm{r.m.s}} B(z) \mathrm{e}^{i\omega_0 t},$$
$$s(z, t) = s_0(z) \mathrm{e}^{i\omega_0 t},$$

where $I_{r.m.s}$ is the current passed through the wire at frequency $\omega_0 = 2\pi\nu$. Then, taking a time average over a period,

$$\overline{v^2} = \omega_0^2 \int_0^l B(z)\,dz \int_0^l B(z')\,dz'\,\mathrm{Re}\{\tfrac{1}{2}s_0(z)s_0^*(z')\}.$$

We expand $s_0(z)$ similarly to above as

$$s_0(z) = \sum_{n=1}^{\infty} A_n\psi_n(z).$$

Whence, from equation (8) and the orthonormality property, we obtain

$$A_n = \frac{\sqrt{2}I_{r.m.s.}}{W_n(\omega_0)}D_n.$$

If ω_0 equals the damped natural frequency of mode n and $\eta \ll 1$, $s_0(z) \simeq A_n\psi_n(z)$ and hence

$$\overline{v^2} = \frac{\omega_0^2 I_{r.m.s.}}{|W_n(\omega_0)|^2}D_n^4.$$

If $\overline{v^2}$ and $|W_n(\omega_0)|^2$ are the same in cases II and III, we have

$$f_{r.m.s.} = \frac{I_{r.m.s.}}{\sqrt{I_c}}D_n. \tag{9}$$

The ergodic hypothesis has been used to equate ensemble with time averages.

Relation (9) forms the basis of the comparison technique. If I_c is known independently, the current necessary to drive the wire at resonance to the same displacement as that caused by a periodic wake at a shedding frequency equal to the resonance frequency determines the sectional r.m.s. lift. A harmonic analysis of the flux per length $B(z)$ is the only additional information required. It is obviously good experimental procedure to arrange permanent magnets providing $B(z)$ in such a way as to augment the response of the mode under study.

Two experimental freedoms may be noted. First, only a minor modification of the analysis is required if different flux fields are used in cases II and III. Second, the flux field may be dispensed with in case II and the voltage comparison can be replaced by a comparison of an end support acceleration in the lift direction, since the force F of the wire on the end support at $z = 0$ in the lift direction is

$$F \simeq T\frac{\partial s}{\partial z}(0,t)$$

and the transfer impedance from $z = 0$, to the accelerometer is the same in both cases.

4. TEST APPARATUS

4.1. WIND TUNNEL

The flow facility used in this investigation is the low-noise, low-turbulence wind tunnel in the Acoustics and Vibration Laboratory at M.I.T. The test section of this wind tunnel provides a 15-in. square open-jet, 22 in. long. The center-line velocity in the open jet ranges between 1 and 65 m/sec with an axial r.m.s. turbulence level of 0·04% of mean velocity at 31 m/sec. The test section is enclosed in a sound-isolated concrete chamber with sound-absorbing treatment on walls, floor and ceiling. Complete characteristics of the wind tunnel are described by Hanson [21].

4.2. TEST RIG

As shown in Figure 1, the test rig holds a cylinder in tension vertically in the open-jet flow by two cantilever arms spaced so that only the cylinder is in the flow. The cylinder is exposed to uniform flow of very low turbulence level except within about 1·25 in. from either end support where there is some disturbance from the low-velocity turbulent free shear layers. Tension is controlled by a turn-buckle on the lower arm. Clamps on each cantilever arm hold the cylinder in place and either provides a flat surface on which to mount an accelerometer with principal axis of sensitivity in the direction of oscillatory lift.

A magnetic field is provided by permanent magnets placed outside the open-jet flow and oriented such that the flux lines are parallel to the flow stream at the cylinder. The cylinder vibrating in the lift direction therefore cuts normally across the lines of flux. The number of magnets and the polarity can be changed to augment the response of any desired mode.

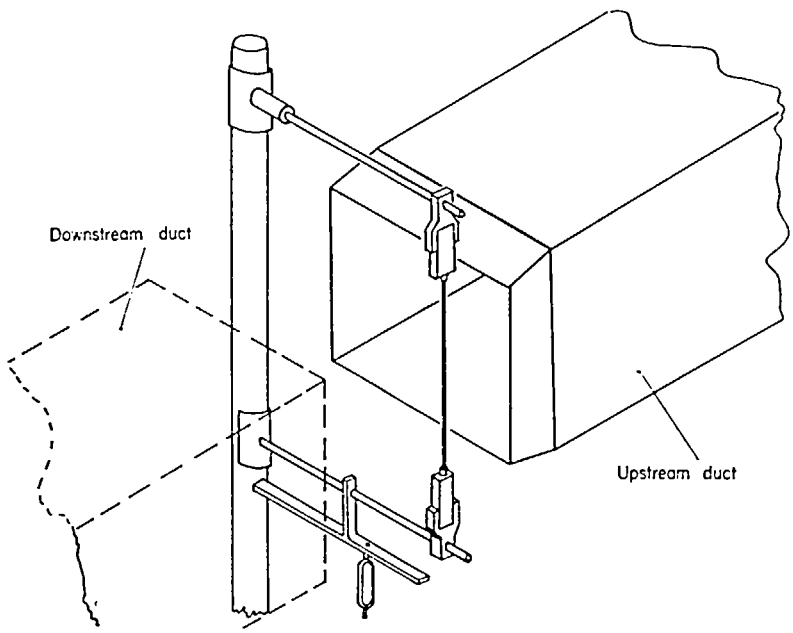

Figure 1. Aeolian tone test rig.

Each magnet has a flux intensity of 1·4 kgauss at the center of a 1·75 in. gap. The flux distribution along the wire is essentially a pure sinusoid and is uniform transversely within the amplitude range of wire motion.

The test cylinder consists of a piano wire 0·091 in. in diameter and an insulated strand of fine magnet wire within a Teflon covering of 0·154 in. outside diameter. The Teflon cover fits tightly around the inner wires and maintains external diameter to within $\pm 0{\cdot}5\%$ even when the piano wire is under considerable tension. The outside surface is free from scratches and is kept clean by wiping with an acetone solution before each experiment.

The piano wire and the fine magnet wire connect to the two separate electrical circuits shown in Figure 2. A sinusoidal current from the oscillator and the power amplifier passes through the piano wire. The force which arises from this alternating current in the permanent magnet field causes the cylinder to oscillate in the desired mode. In turn, the voltage induced in the fine wire by cylinder oscillation in the magnetic field is displayed and measured on an oscilloscope. Compensation for the voltage induced in the fine wire from its proximity to

the parallel current-carrying wire is carried out by winding their connecting leads in opposite directions around a common air core.

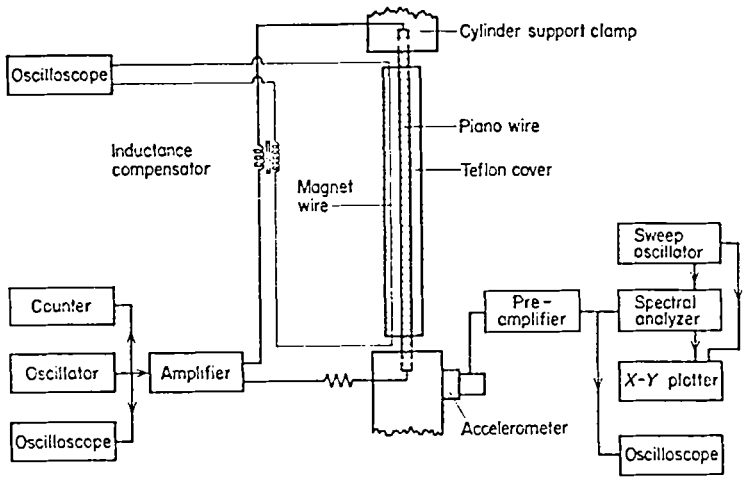

Figure 2. Schematic of experimental apparatus.

4.3. TRANSDUCERS AND EQUIPMENT FOR ANALYSIS

The transducers for measuring end-support acceleration, radiated sound pressure level and wake velocity structure are a Brüel and Kjær accelerometer, type 4332, a Brüel and Kjær 1 in. condenser microphone, type 4131 and two DISA, type 55A22, constant temperature hot-wire anemometer probes, respectively. The associated instrumentation is a Brüel and Kjær cathode follower for the microphone and the accelerometer and two DISA constant temperature anemometer units, type 55D05, for the hot-wire probes.

Equipment for analysis is a Brüel and Kjær frequency analyzer, type 2107, for constant percentage bandwidth spectrum analysis, a Spectral Dynamics spectral analyzer, type SD 101A with 5 Hz bandwidth and a Princeton Applied Research correlation function computer, model 100.

5. MEASUREMENT PROGRAM

5.1. RADIATED SOUND PRESSURE LEVEL AND DIRECTIVITY

The cylinder in tension was placed in the open-jet test section within the anechoic chamber. As the flow velocity past the cylinder increased, the discrete Aeolian tone became unmistakable. With the microphone on a swinging boom pivoted beneath the cylinder on axis, the radiated sound pressure level was measured at distances of 6, 12, 18, 24 and 36 in. from the center of the cylinder on the x-axis (see Figure 4) and at 15° and 30° off axis. The microphone signal was analyzed by the Brüel and Kjær wave analyzer with a 6% bandwidth filter. Some of the recorded spectra are shown in Figure 3, where the peaks at the shedding frequencies are evident. The sound intensity of the Aeolian tone at these frequencies is shown in Figure 4 as a function of velocity.

Dipole directivity with axis in the cross-flow direction of oscillatory lift was determined within the angular limits of $\pm$ 30° from axis fixed by the presence of upstream and downstream ducting. A slight reduction of sound pressure level of about 1 dB was measured, confirming expectations. The wire had been tested previously in another low-turbulence wind tunnel

which lacked an anechoic chamber but had no downstream duct to cause interference. There we were able to confirm qualitatively the strong dipole directivity with axis, that of oscillatory lift.

The microphone was also traversed parallel to the wire at a distance of 6 in. from the wire in the direction of the oscillatory lift dipole axis. Sound pressure level reductions of approximately 3 dB from the mid-span level were obtained when the microphone was opposite

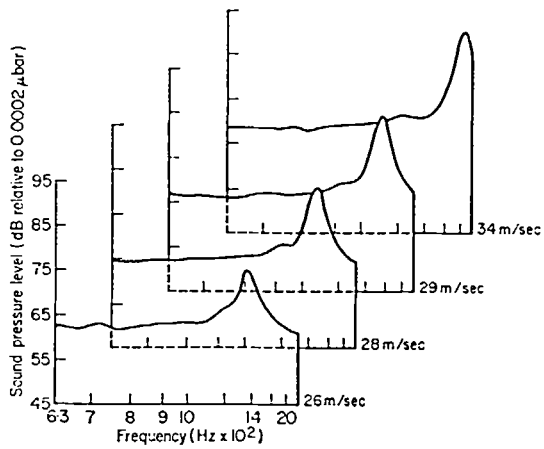

Figure 3. Six percent bandwidth radiated sound levels at a distance of 17 in. from the cylinder.

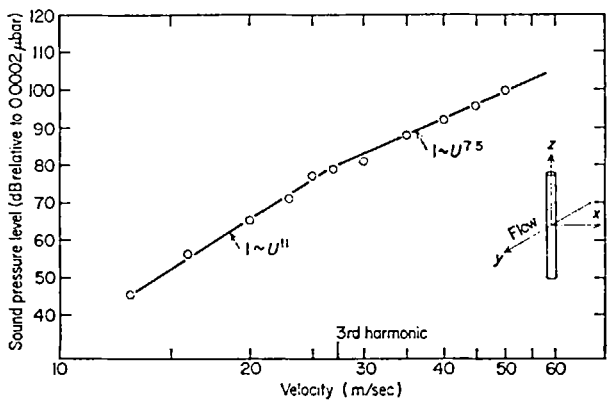

Figure 4. Sound intensity at shedding frequency measured at $x = 12$ in. Dimensions of cylinder are 0·154 in. × 15 in.

either end of the wire. These reductions are what one would expect from a distribution of uncorrelated dipoles along the wire, each of length equal to the correlation length l_c of vortex shedding reported in section 5.4 following.

No significant standing wave effects were found in the anechoic chamber. The calibration of this chamber by a sound source placed at the wire location is shown in Figure 11. Spherical spreading loss existed for the frequencies and distances used in these experiments.

5.2. END SUPPORT ACCELERATION

With the cylinder still in position in the flow, an accelerometer was mounted on the lower support clamp with its sensitive axis aligned with oscillating lift. The end support acceleration response was displayed visually on an oscilloscope and was recorded in the form of a

spectrum by either the Brüel and Kjær 6% bandwidth wave analyzer or the Spectral Dynamics analyzer with 5 Hz bandwidth. For example, the acceleration response at a number of velocities shown in Figure 5 was obtained with the 6% bandwidth filter. The vortex shedding frequency marked S was clearly discernible as well as each of the first three harmonic resonances of the cylinder, marked 1, 2 and 3. The peak labeled F was caused by a structural excitation not related to the flow excitation and hence ignored.

The investigation of a possible "lock-in" effect as the vortex shedding frequency approached and passed through a harmonic resonance of the cylinder was accomplished by sweeping the 5 Hz bandwidth spectral analyzer very slowly through the frequencies containing both peaks at each of several increments of velocity. The plots shown in Figure 6 were the results of this procedure near the third harmonic resonance of the cylinder.

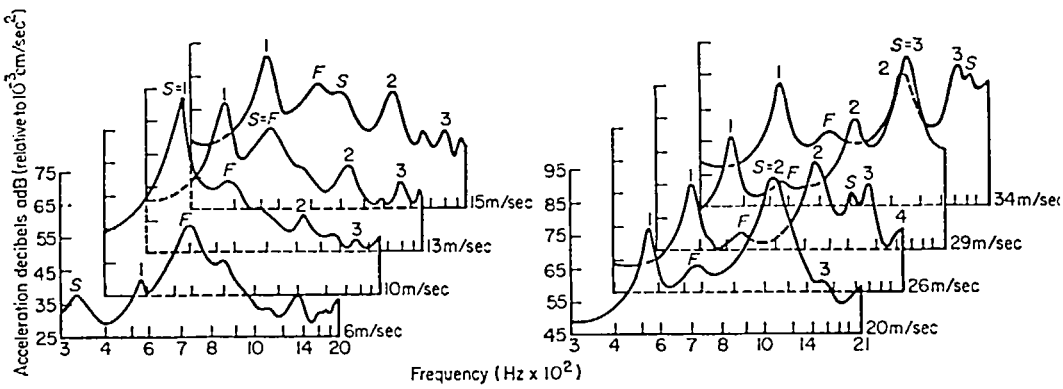

Figure 5. Six percent bandwidth end-support acceleration levels.

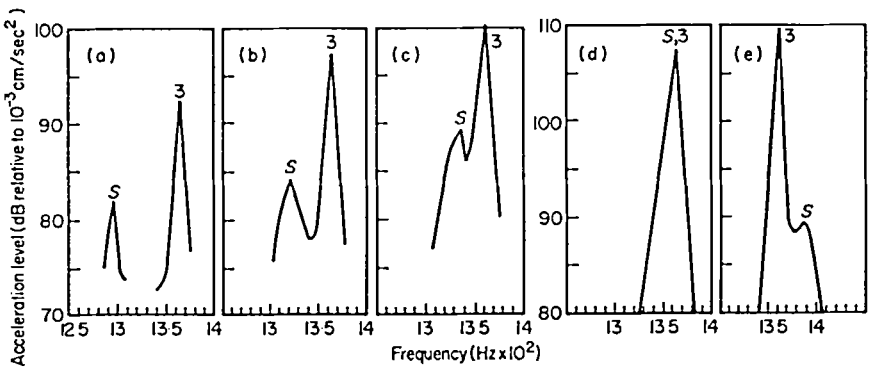

Figure 6. Five Hz bandwidth end-support acceleration levels showing the shedding frequency passing through the third harmonic resonance frequency. Velocities equal (a) 24·2 m/sec, (b) 24·7 m/sec, (c) 24·9 m/sec, (d) 25·2 m/sec, (e) 26·0 m/sec.

5.3. COMPARISON TECHNIQUE

In the discussion of the comparison technique earlier, it was pointed out that the lift force on the wire could be measured by a voltage comparison method or by an end-support acceleration method. Both methods were used with good results.

5.3.1. *Acceleration comparison method*

With the cylinder in air flow, the end-support acceleration was obtained at coincidence of shedding frequency with one of the harmonic resonance frequencies of the cylinder. Then the

flow was stopped and was replaced by a magnetic flux field. A current at the frequency of resonance was passed through the piano wire at a level which gave the same end-support acceleration level as was obtained in flow. After measuring the flux field intensity along the cylinder with a rotating coil gauss-meter, the r.m.s. force was determined using the method outlined in section 3.

5.3.2. *Voltage comparison method*

While using this procedure, it was necessary to place the magnets just outside the open jet so that the magnets did not disturb the flow. As described in section 4, the fine wire within the cylinder was connected to an oscilloscope. Once again the flow velocity was adjusted so that coincidence between shedding frequency and cylinder resonance frequency occurred. As the cylinder oscillated in the lift direction, a voltage was induced in the fine wire and was measured on the oscilloscope. Then the flow was stopped and a current at the same frequency was sent through the piano wire, causing it to vibrate in the magnetic field. The current was adjusted so that the voltage induced in the fine wire matched its previous level under flow. Once again the force on the wire was calculated from the known current value and the measured flux field.

Here we ran into the practical difficulty of obtaining the same flux fields under flow and under no-flow conditions. The analysis leading to equation (9) was suitably modified to obtain, for the r.m.s. force,

$$f_{\text{r.m.s.}} = \frac{I_{\text{r.m.s.}}}{\sqrt{l_c}} \frac{D^2_{n(2)}}{D_{n(1)}},$$

where subscript 1 refers to conditions under flow and subscript 2 refers to conditions under no flow, and the subscript n refers to the number of the mode being resonantly excited.

5.4. LATERAL SPATIAL CORRELATION OF SHED VORTICES

This series of measurements was concerned with the effective correlation length of the shed vortices. As shown in Figure 7, two hot-wire anemometer probes, one fixed and one movable, were placed in the wake of the cylinder to obtain the longitudinal component of fluctuating velocity. The probes were positioned by traversing across and along the wake until the signals showed both a sinusoidal wave form and the maximum r.m.s. velocity on a dual channel oscilloscope.

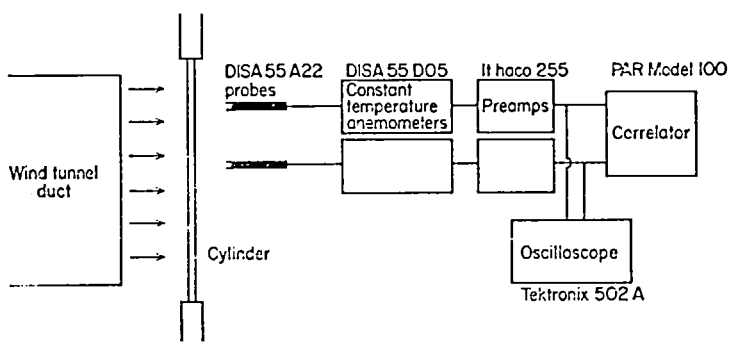

Figure 7. Apparatus used for determination of correlation length.

The output signals from the DISA anemometer units were then amplified by two Ithaco 255-A preamplifiers and the normalized cross-correlation was obtained using a Princeton Applied Research model 100 correlator.

After finding the optimum position for one probe, the other was brought as close to it as possible without actual contact while keeping a vertical alignment parallel to the cylinder axis. Alignment was checked by measuring directly the positions of the probes and also by checking the autocorrelation function of each signal at various positions. A safe working distance was 0·0625 in. center-to-center of the 1-mm long hot wires. The correlation coefficient was obtained for this spacing, after which the movable probe was raised to a new position. A typical correlation curve is shown in Figure 9.

From the plot of lateral spatial correlation coefficient the correlation length l_c and the centroid γ were determined. The correlation length was the area under the curve:

$$l_c = 2\int_0^\infty R(\xi)\,d\xi,$$

and the centroid γ was related to the moment of positive area under the curve by

$$\gamma = \frac{2}{l_c}\int_0^\infty \xi R(\xi)\,d\xi.$$

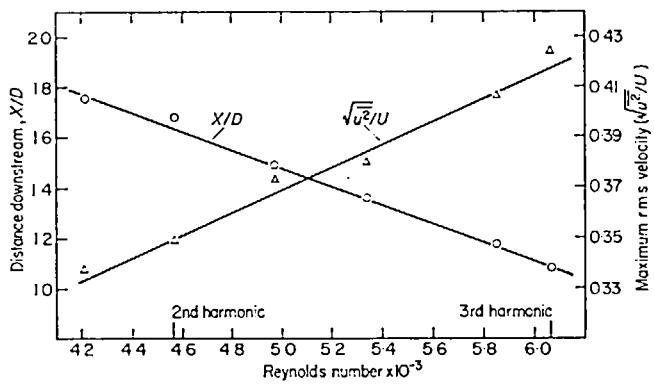

Figure 8. Downstream distance from cylinder center and amplitude of maximum r.m.s. velocity (Ballou [24]).

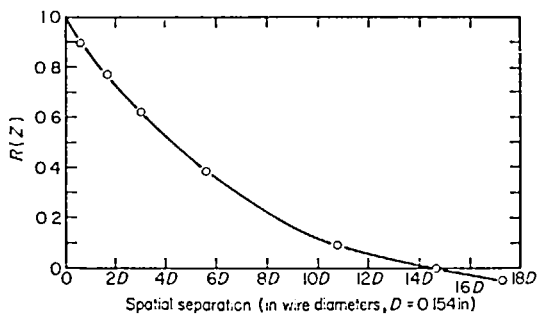

Figure 9. Lateral spatial correlation coefficient of fluctuating longitudinal velocity in wake of cylinder at Re D = 6·05 × 10³.

The lateral spatial correlation curve was unchanged for various positions along the cylinder to within 1·25 in. from an end where the cylinder was immersed in the shear layer of the open jet. Correlation curves were obtained at several flow speeds with resulting values of l_c and γ tabulated in Table 2. No significant influence of coincidence of shedding with resonant frequency upon l_c or γ was observed as shown in the plot of l_c vs. Reynolds number in Figure 10.

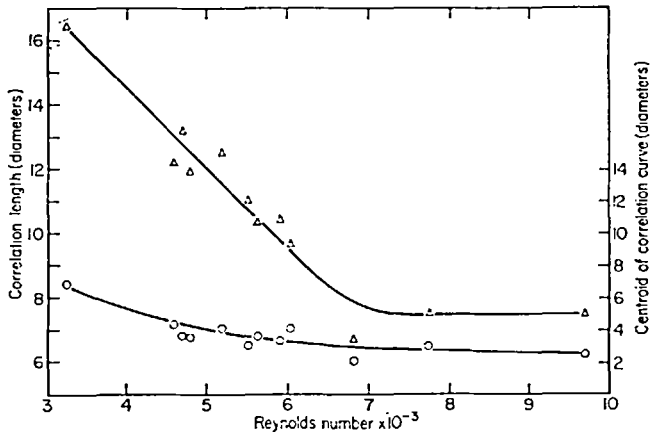

Figure 10. Lateral spatial correlation length and centroid of positive correlation area as a function of Reynolds number. △——△, correlation length; ○——○, centroid.

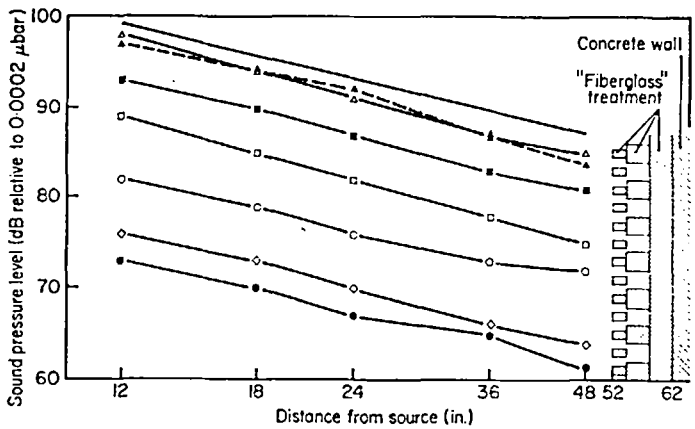

Figure 11. Calibration of anechoic chamber. Third octave bands: △——△, 2000; ▲——▲, 4000; □——□, 1000; ■——■, 8000, 10,000; ○——○, 50; ●——●, 315; ◇——◇, 16,000. ——, Free field.

5.5. DAMPING MEASUREMENT

The quality factor $Q = 1/\eta$ at each resonance was determined with no mean flow. This was done by measuring decay rates of the vibration after excitation was suddenly stopped. The excitation was provided once again by current at resonance frequency through the piano wire immersed in a magnetic flux field. Current was stopped by a micro-switch and the vibration decay rate was observed from the decaying signal from an accelerometer on the end supports. The results are shown in Table 1.

TABLE 1
Results of damping measurements

Harmonics	Hz	$Q = 1/\eta$
1	470	515
2	923	420
3	1387	1387
4	1863	1950

These values of Q are considered sufficiently high that only the mode in question is excited significantly.

5.6. CYLINDER DISPLACEMENT

The displacement of the cylinder under flow excitation in the presence of a known magnetic field was determined from measuring the voltage induced in the fine wire. Using the expression

$$v(t) = -\int_0^l B(z)\frac{\partial s}{\partial t}(z,t)\,dz,$$

a straightforward harmonic analysis yields the r.m.s. displacement as a function of the r.m.s. voltage induced in the fine wire, the frequency, the length of the wire, and the harmonic component of the B-field.

By this method, we obtained a displacement at third harmonic resonance of $s_{r.m.s.} = 3{\cdot}03 \times 10^{-3}$ in. The peak single amplitude displacement to diameter ratio was $s_{peak}/d = 2{\cdot}8\%$.

6. DISCUSSION AND CONCLUSIONS

Measurements of oscillating lift coefficient, spanwise correlation length, Strouhal number and radiated sound intensity were made on the same cylinder under the same test conditions over a Reynolds number range of 4000 to 6450. Additional spanwise correlation lengths were measured over a Reynolds number range of 3000 to 9700. These measured values were then used as terms in equation (3) for the intensity radiated from a cylinder in a flow field and this predicted intensity was compared with the actual measured value. The comparison and tabulation of all the results are given in Table 2.

TABLE 2

Summary of measured and predicted values

Reynolds number (Ud/ν)	r.m.s. sectional lift coefficient	Correlation length (diameters)	Centroid of correlation (diameters)	Predicted intensity at $r = 36$ in. (dB)	Measured intensity at $r = 36$ in. (dB)
4000	0·04	15·0	5·2	47	46
4090	0·03	13·0	4·0	46	46
4140	0·08	12·5	4·0	55	54
6050	0·42	9·7	3·7	78	76
6260	0·43	9·2	3·5	79	77
6450	0·51	8·5	3·2	80	77

The agreement between the measured and the predicted intensity serves to verify (3) for the dipole sound radiation from a cylinder in a flow field. The comparison was made at $x = 36$ in. from the center of the cylinder. At this distance the directivity effect of the cylinder acting as a 15-in. long distribution of uncorrelated dipoles requires negligible correction.

The results show that the oscillating lift coefficient is the controlling factor in the radiated sound intensity. In the Reynolds number range of this investigation, the rise in intensity level with velocity is accompanied by a sharp increase in the lift coefficient while the spanwise correlation length decreases steadily. We observe little dependence of the correlation length on resonance of the cylinder and no sign of "lock-in" of the shedding frequency with vibrating frequency. As shown in Figure 6, we were able to separate shedding frequency and resonant

frequency within 2%. These results are likely due to the vibration amplitude of 3% of the cylinder diameter at resonance being insufficient to cause any increase in the correlation length. It is felt that the phenomenon of "lock-in" accompanied by large increases in correlation length is observed only in cases where there is considerable amplitude of vibration.

The lift coefficient increase corresponds to that found by Gerrard [5] in this Reynolds number range. It is significant that this result is found in two investigations which use very low-turbulence wind tunnels. This is an indication that any destabilizing influence such as upstream turbulence or cylinder vibration increases the lift coefficient. This is likely due to the decrease in the length of the formation region and perhaps an increase in the vortex strength from such an influence. The measurements shown in Figure 8 tend to confirm this. In Figure 8, we show the downstream distance from the cylinder to the position of maximum r.m.s. velocity which is a direct measure of the length of the formation region. The length decreases linearly with an increase in Reynolds number, a result which agrees with the measurements of Bloor [22] in this Reynolds number range. Moreover, the amplitude of the maximum r.m.s. longitudinal velocity component increases linearly with Reynolds number (Ballou [24]). This suggests an increase in vortex strength, although Bloor and Gerrard [25] caution against such an interpretation. It should be emphasized, however, that the vibration amplitude of our cylinder increases to a maximum at the third harmonic resonance which occurs at the upper end of this Reynolds number range, hence our results should be somewhat different from those obtained for rigid cylinders.

Measurements of the sound intensity radiated from the cylinder excited by motor action alone were 25 dB lower at $x = 12$ in. than those radiated in flow with the same vibration amplitude in each case. Also, the radiated sound spectrum in Figure 3 shows a peak only at the Strouhal frequency and at none of the cylinder harmonic resonances. Moreover, the analysis in Appendix I shows that in this case the sound radiation from vibration alone is largely end-fire and, as such, does not enter into the dipole radiation of cylinder in flow. Thus the vibration of the cylinder alone does not contribute significantly to the radiated sound.

ACKNOWLEDGMENT

We wish to acknowledge Naval Ship Research and Development Center and Office of Naval Research sponsorship, the help of Mr Hugh Ching on test rig design, including the concept of the comparison technique, and the work of Lt Charles Ballou, U.S. Navy, on the measurements of the near wake.

REFERENCES

1. M. J. LIGHTHILL 1952 *Proc. R. Soc. A* **211**. On sound generated aerodynamically. I. General theory.
2. N. CURLE 1955 *Proc. R. Soc. A* **231**. The influence of solid boundaries upon aerodynamic sound.
3. O. M. PHILLIPS 1956 *J. fluid Mech.* **1**. The intensity of Aeolian tones.
4. LORD RAYLEIGH 1896. *The Theory of Sound*, Vol. II. New York: Dover Publications.
5. J. H. GERRARD 1961 *J. fluid Mech.* **11**, 224. An experimental investigation of the oscillating lift and drag of a circular cylinder shedding turbulent vortices.
6. C. GRAHAM 1966 *M.I.T. Acoust. Vib. Lab. Rep.* 76028-1. A survey of correlation length measurements of the vortex shedding process behind a circular cylinder.
7. G. H. KOOPMAN 1967 *J. fluid Mech.* **28**, 501. The vortex wakes of vibrating cylinders at low Reynolds numbers.
8. N. FERGUSON and G. V. PARKINSON 1967 *ASME Paper No. 67-Vibr-31*. Surface and wake flow phenomena of the vortex-excited oscillation of a circular cylinder.
9. R. E. D. BISHOP and A. Y. HASSAN 1964 *Proc. R. Soc. A* **277**, 51. The lift and drag forces on a circular cylinder oscillating in a flowing fluid.
10. E. BERGER 1967 *Phys. Fluids Suppl.* Suppression of vortex shedding and turbulence behind oscillating cylinders.

11. M. J. LIGHTHILL 1962 *Proc. R. Soc. A* **267**, 147. The Bakerian lecture. Sound generated aerodynamically.
12. H. M. FITZPATRICK and M. STRASBERG 1957 *Naval Hydrodynamics Publication* 515 *Nat. Acad. Sciences: Washington, D.C.* Hydrodynamic sources of sound.
13. R. T. KEEFE 1961 *UTIA Rep.* 76. An investigation of the fluctuating forces acting on a stationary circular cylinder in a subsonic stream and of the associated sound field.
14. L. S. G. KOVASNAY 1949 *Proc. R. Soc. A* **198**, 174. Hot-wire investigation of the wake behind cylinders at low Reynolds numbers.
15. V. PRENDERGAST 1958 *UTIA tech. Note* 23. Measurement of two-point correlations of the surface pressure on a circular cylinder.
16. M. Y. EL BAROUDI 1960 *UTIA tech. Note* 31. Measurement of two-point correlations of velocity near a circular cylinder shedding a Kármán vortex street.
17. G. H. KOOPMAN 1969 *Dissertation, Catholic University of America.* Wind induced vibrations and their associated sound fields.
18. G. K. BATCHELOR 1967 *An Introduction to Fluid Dynamics.* Cambridge University Press.
19. J. W. MILES 1965 *J. acoust. Soc. Am.* **38**, 855. Stability for forced oscillations of a vibrating string.
20. H. CRAMÉR and M. R. LEADBETTER 1967 *Stationary and Related Stochastic Processes.* Chapter 7. New York: Wiley.
21. C. E. HANSON 1968 *M.I.T. Acoust. Vib. Lab. Rep.* 79611-1. The design, development and construction of a low-noise, low-turbulence wind tunnel.
22. M. S. BLOOR 1964 *J. fluid Mech.* **19**, 290. The transition to turbulence in the wake of a circular cylinder.
23. D. T. LAIRD and H. COHEN 1952 *J. acoust. Soc. Am.* **24**, 46. Directionality patterns for acoustic radiation from a source on a rigid cylinder.
24. C. L. BALLOU 1967 *M.I.T. Acoust. Vib. Lab. Rep.* 76028-2. Investigation of the wake behind a cylinder at coincidence of a natural frequency of vibration of the cylinder and the vortex shedding frequency.
25. M. S. BLOOR and J. H. GERRARD 1966 *Proc. R. Soc. A* **294**, 319. Measurements on turbulent vortices in a cylinder wake.

APPENDIX I

RADIATION FROM A VIBRATING CYLINDER IN AN INFINITE CYLINDRICAL BAFFLE

Our analysis follows that of Laird and Cohen [23], hence we shall only outline the steps. We assume no deformation of a cylindrical cross-section of radius a and small vibration of its axis in an odd standing wave mode

$$v = \frac{\partial s}{\partial t} = v_m \cos(k_m z)\, e^{-i\omega t}, \qquad |z| < \frac{l}{2},$$

$$= 0, \qquad |z| > \frac{l}{2},$$

where $k_m = (2m-1)\pi/l$, $m = 1, 2, \ldots$.

The acoustic pressure p must satisfy the wave equation and the matching boundary condition in cylindrical (r, ϕ, z) co-ordinates

$$\left.\frac{\partial p}{\partial r}\right|_{r=a} = i\omega\rho_0 v \cos\phi.$$

Suppressing the factor $\cos\phi\, e^{-i\omega t}$ we find readily that

$$p(r,z) = \frac{(-1)^{m+1}}{\pi} i\omega\rho_0 v_m k_m \int_{-\infty}^{\infty} e^{ikx} \frac{\cos(kl/2)}{k_m^2 - k^2} \frac{H_1^{(1)}(\kappa r)\, dk}{\kappa H_1^{(1)\prime}(\kappa a)}, \tag{A1}$$

where $H_1^{(1)}$ is the Hankel function of first kind of first order and

$$\kappa = \sqrt{k_0^2 - k^2} (\to k_0 \text{ as } k \to 0), \qquad k_0 = \omega/c_0,$$

with c_0 the sound speed.

We obtain the far-field pressure by converting to spherical co-ordinates (R,ϕ,θ), where $z = R\cos\theta$, $r = R\sin\theta$, and applying the method of stationary phase to (A1). For $k_0 R \gg 1$ we have

$$p(R,\theta) \simeq \frac{(-1)^m i}{2} \rho_0 c_0 v_m \frac{k_0^2 a^2}{R} k_m \sin\theta \frac{\cos(k_0 l/2)\cos\theta}{k_m^2 - k_0^2\cos^2\theta}. \tag{A2}$$

For $k_m < k_0$, $|p(R,\theta)|$ has maxima at $\theta_0 = \arccos(k_m/k_0)$ and at $\pi - \theta_0$. Resolving the indeterminate form, we find the intensity I of radiation at these angles to be

$$I(R,\phi,\theta_0) = \frac{|p^2|}{2\rho_0 c_0}$$
$$= \frac{\rho_0 c_0}{128}\left(v_m \frac{l\sin\theta_0\cos\phi}{R}\right)^2 (k_0 a)^4. \tag{A3}$$

A typical example from our experiments is the resonant excitation of the wire third harmonic by current drive to an r.m.s. displacement of 3 % of wire diameter. Numerical values are

$$\omega/2\pi = 1400 \text{ Hz}, \qquad R = 2 \text{ ft},$$
$$l = 15 \text{ in.}, \qquad v_2 = 1{\cdot}48 \text{ m/sec},$$
$$2a = 0{\cdot}154 \text{ in.}, \qquad \rho_0 c_0 = 415 \text{ MKS rayls}.$$

For these conditions $k_2 = 24{\cdot}5 \text{ m}^{-1}$, $k_0 = 25{\cdot}6 \text{ m}^{-1}$ and $\theta_0 = 4° 48'$. The radiation is thus essentially end fire along the cylinder axis. At $\theta = \theta_0$ and $\cos\phi = 1$ the intensity I is $1{\cdot}5 \times 10^{-7}$ w/m^2, corresponding to a sound pressure level of 52 dB (relative to 0·0002 dynes/cm^2).

An estimate of the radiation damping is also possible. The power radiated is

$$\frac{1}{2\rho_0 c_0}\int_0^{2\pi} d\phi \int_0^{\pi} d\theta R^2 \sin\theta |p|^2 = \frac{\pi}{8}\rho_0 c_0 (v_m k_m)^2 (k_0 a)^4 \int_0^{\pi} \sin^3\theta \left(\frac{\cos(k_0^l/2)\cos\theta}{k_m^2 - k_0^2\cos^2\theta}\right)^2 d\theta. \tag{A4}$$

A crude upper bound on the integral in (A4) is $\pi l^2/16k_m^2$. Alternatively, the power radiated is

$$\tfrac{1}{2} r_c \int_{-l/2}^{l/2} |v|^2 \, dx = \tfrac{1}{4} r_c v_m^2 l, \tag{A5}$$

where

$$r_c = \rho_b \pi a^2 \eta\omega \tag{A6}$$

is the radiation damping coefficient, ρ_b is the wire density and η is the radiation loss factor.

Comparing (A4) with (A5) and (A6) we obtain the bound on the quality factor $Q = \eta^{-1}$:

$$Q > \frac{32}{\pi}\frac{\rho_b}{\rho_0} l k_0^3 a^2. \tag{A7}$$

Using the numerical values of parameters given above and $\rho_b = 4060$ kg/m^3 as the average density of our cylinder, we get

$$Q > 1{\cdot}32 \times 10^6,$$

signifying negligible radiation damping.

APPENDIX II

ESTIMATE OF THE VISCOUS DAMPING OF AN OSCILLATING CYLINDER

Batchelor [17, p. 357] extending earlier work by Stokes and Schlichting, obtained the quality factor

$$Q = \frac{a\rho_b}{\rho_0}\left(\frac{\omega}{8\nu}\right)^{1/2}$$

for a cylinder of radius a and density ρ_b oscillating in a viscous incompressible fluid at frequency ω. His solution is valid to first order in the ratio of amplitude of vibration to cylinder diameter. Equal contributions to the damping force were found from the tangential and normal stresses.

It is evident that this solution must be valid for any mode of resonant vibration. Using numerical values of the parameters for the example of Appendix I together with $\nu = 1{\cdot}5 \times 10^{-5}$ m^2/sec, we obtain $Q \simeq 6 \times 10^4$. This value is about 60 times greater than the measured values of Q reported in section 5.5.